SAND96-2972C
CONF-9706113--3

INDUCTIVE VOLTAGE ADDER (IVA) FOR SUBMILLIMETER RADIUS ELECTRON BEAM

M. G. Mazarakis, J. W. Poukey, J. E. Maenchen, D. C. Rovang, P. R. Menge, J. S. Lash, D. L. Smith, D. L. Johnson, J. A. Halbleib, S. R. Cordova, K. Mikkelson, J. Gustwiller, and W. A. Stygar
Sandia National Laboratories, P. O. Box 5800, Albuquerque, NM 87185

D. R. Welch
Mission Research Corporation, 1720 Randolph Road SE, Albuquerque, NM 87106

I. Smith and P. Corcoran
Pulse Sciences Incorporated, 600 McCormick, San Leandro, CA 94577

Abstract

We have already demonstrated the utility of inductive voltage adder accelerators for production of small-size electron beams. In our approach, the inductive voltage adder drives a magnetically immersed foilless diode to produce high-energy (10-20 MeV), high-brightness pencil electron beams. This concept was first demonstrated with the successful experiments which converted the linear induction accelerator RADLAC II[1] into an IVA fitted with a small 1-cm radius cathode magnetically immersed foilless diode (RADLAC II/SMILE).[2] We present here first validations of extending this idea to mm-scale electron beams using the SABRE[3] and HERMES-III[4] inductive voltage adders as test beds. The SABRE experiments are already completed and have produced 30-kA, 9-MeV electron beams with envelope diameter of 1.5-mm FWHM. The HERMES-III experiments are currently underway.

Introduction

During the last 15 years, Sandia National Laboratories dedicated a considerable effort toward developing ultra high-current and high-brightness electron beams from 4 to 20 MeV and 30 to 100 kA. The accelerators utilized were compact and inexpensive single-pulse devices, which can be divided into two groups: single-stage Blumleins, such as HERMES II[5] and IBEX,[6] and multistage devices, such as RADLAC I,[7] RADLAC II, RADLAC II/SMILE, and MABE.[8]

The electron source used was the magnetically immersed foilless diode,[9] where high-current and high-brightness electron beams are generated and propagated in a strong axial magnetic field, and high currents can be contained in small radial cross sections with relatively small transverse velocities. The primary advantages of this source, in comparison to magnetic field free devices, are its insensitivity to voltage and applied magnetic field variations and its production of high-current, small-radius electron beams in equilibrium, as opposed to beams focused at only one axial location.

The experiments reported here are motivated by the success of converting RADLAC II (an induction linac) into an equal impedance (~ 120-ohm) inductive voltage adder coupled to a magnetically immersed foilless diode (RADLAC II/SMILE). The inductive voltage adder (IVA) technology is relatively simple and couples a self-magnetically insulated transmission line (MITL)[10] with an induction linac[11] to generate a new family of induction accelerators. In these accelerators, the particle beam which drifts through the multiple cavities of conventional induction linacs is replaced by a metal conductor which extends along the entire length of the device. The voltage addition of the accelerating cavities is therefore accumulated in the TEM Poynting vector rather than in a sequentially accelerated electron beam. These devices can operate in either polarity to produce negative or positive voltage pulses. In a negative polarity voltage adder (Fig. 1), the center

conductor is negatively charged relative to the outer conductor which is interrupted at regular intervals by the cavity gaps.

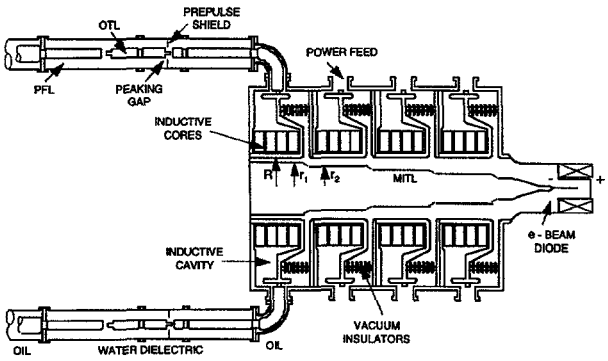

Figure 1. A negative polarity voltage adder of the SABRE type.

The experiments described here utilize the SABRE and HERMES-III inductive voltage adders modified to higher impedance (~ 100 ohms) driving a foilless diode immersed in a very strong (10-50 Tesla) solenoidal magnetic field. A tantalum bremsstrahlung converter is immersed in the same magnetic field and defines the anode of the diode.

In the next sections, we present SABRE and HERMES-III modifications, new IVA cathode and immersed diode designs, numerical validations, and experimental results and analysis. We start first with the SABRE experiments and conclude with a progress report on the HERMES-III experiments.

SABRE Experiments

A. IVA Modifications

SABRE has 10 inductively insulated cavities each rated at 1.2 MV, designed to operate at 40 ohms in negative polarity and at 20 ohms in positive polarity. Ideally, SABRE should produce –12 MV, 300 kA, and +8 MV, 400 kA. Because of higher than expected energy losses in the pulse forming network, the operating input cavity voltage is 700 kV, which limits the total output voltage to ~ 7 MV for negative polarity and 5 MV for positive polarity.

For these experiments, SABRE was modified to increase the output voltage and proportionally reduce the current, delivering the same total energy. SABRE's slow pulsed power section consists of a Marx generator, two intermediate storage capacitors, and two triggered gas switches. Each switch controls the charging of ten pulse forming lines (PFLs). The PFLs charge as capacitors but discharge through self breaking water switches as 7.8-ohm, 40-ns transmission lines, each pair driving a cavity through a bent output transmission line structure (Fig. 1). This fast pulsed power section was modified by halving the number of pulse forming and transmission lines (from 20 to 10), feeding each cavity only from one side.

Halving the fast pulsed power section substantially increased the intermediate store, pulse forming line ringing ratio, providing a 50% higher voltage to the transmission lines and cavities (~ 1.0 MV). To take advantage of and to maintain the voltage gain, the voltage adder impedance was also increased by constructing a smaller diameter cathode electrode. Normally, the impedance of the voltage adder is matched to that of the cavities; however, to maintain a margin for further increasing the output voltage, the voltage adder impedance was built 40% higher. The transfer

switches were adjusted to close at 2.2 MV, instead of the usual 2.6 and 2.8 MV, to avoid exceeding 1.2 MV per cavity.

The high-impedance cathode electrode for the voltage adder was designed utilizing the formalism developed by Ref. 2. A photograph and a scale drawing of the cathode electrode is shown in Fig. 2. A stepped geometry was selected for SABRE where the constant radius segments provide constant vacuum impedance. The impedance increases at a rate which follows the axial voltage gradient along the feed. The latter assures constant current flow over the entire length of SABRE and evanescent reverse directed electromagnetic waves. The cathode electrode, including the voltage adder section (6 m long) and a constant radius extension section (3.6 m long), is cantilevered from the low-voltage end of the accelerator. It starts with a 13.65-cm radius cylinder at the grounded end and tapers to 2.2-cm radius after the 10th cavity. Nine conical tapers were utilized along with 10 cylindrical sections and 11 flex-adjusting, double-washer sections preloaded to compensate for gravitational droop. Because of the large difference in radius between the surrounding anode and the cathode cantilever, precise alignment and centering is not critical since the electrical potential is a logarithmic function of the radii. Precise alignment is, however, required at the diode end, and the cantilevered cathode is adjusted *in situ* to center the high-voltage end.

B. Immersed Diode Design

The magnetically immersed foilless diode is similar to that of RADLAC II/SMILE. However, SABRE diode impedance and solenoidal magnetic field are much higher, and the cathode in the diode is a needle on the axis (Figs. 1 and 2), unlike the annular diode in RADLAC II. To generate beams of millimeter sizes, the diode must be immersed in solenoidal fields of 20-50 T.[11-12] Figure 3 shows a schematic diagram of the diode design, including the solenoidal magnet. The shape of the fringe field is tailored by a 2-cm thick aluminum cylinder of 25-cm inner radius coaxially enclosing the entire diode assembly.

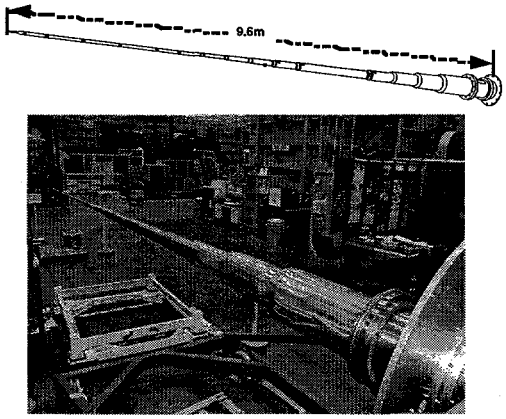

Figure 2. IVA and extension MITL cathode electrode.

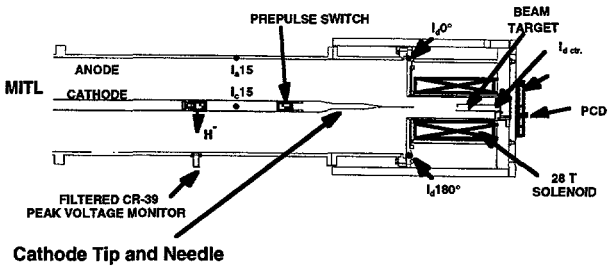

Figure 3. Schematic diagram of diode design and transition region, showing details and diagnostics.

This diode design was operated at up to 20 T field. A half length coil was utilized to reach ~ 30 T field. These solenoids are among the strongest ever built. The total magnetic energy stored is ~ 1.8 MJ in an 8-16-mH inductance, providing a working bore of 12 cm. The 20-T coils are 30-cm long while the 30-T coils are half as long. The SABRE solenoids were designed and constructed at Sandia, drawing upon the extensive inertial confinement fusion ion beam electromagnet experience. The diode walls and cathode conical section are made of titanium for its strength, nonmagnetic, and large resistivity properties, allowing the pulsed field to penetrate without appreciable losses.

C. Design Validation with Numerical Simulations

The design of the MITL voltage adder and the foilless diode were validated with a large number of TWOQUICK[13] particle-in-cell simulations. Because of the large range in space and time scales, the entire design was divided into three parts: the voltage adder (Fig. 4); the transition region, where the coupling from the MITL into the immersed diode was studies (Fig. 5); and finally, the immersed diode where the beam generation and beam parameters were analyzed in fine detail (Fig. 6). The diode simulations (Figs. 5 and 6) represent an ideal situation assuming no ion emission from the target, perfect cylindrical symmetry, and no instabilities between counterstreaming electrons and ions.

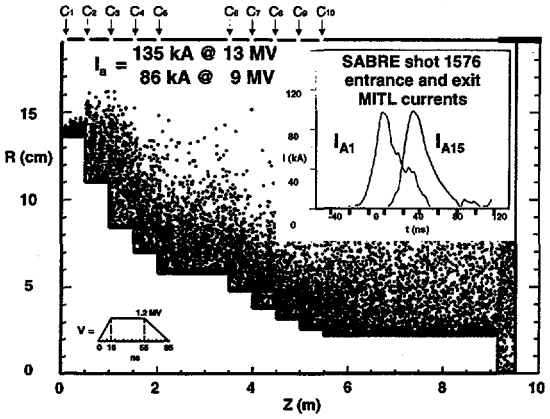

Figure 4. IVA simulations are in very good agreement with experimental results. I_{A1} is the total current measured at the beginning (near C_1) of the IVA and I_{A15} at the end of the MITL.

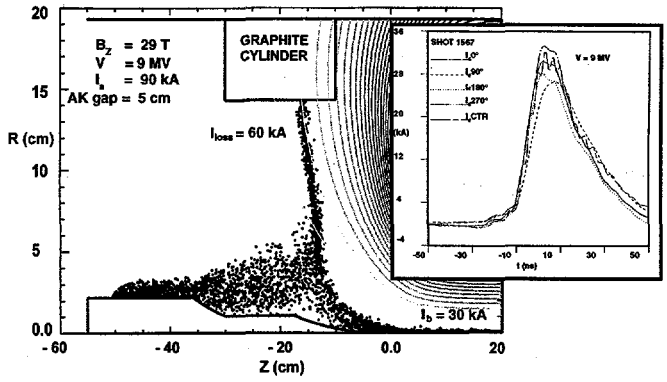

Figure 5. Simulations of the transition region predicted quite well the diode beam currents. I_{d0° -I_{270° and I_{dCTR} are the beam current measured with the five $\dot{B}$ monitors of the diode.

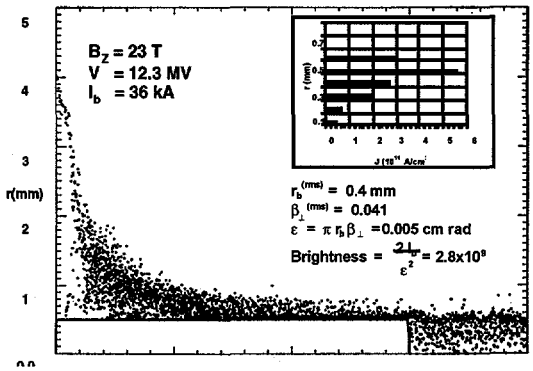

Figure 6. High-resolution diode simulation calculating the beam parameters.

D. Experimental Results

The experimental results are in full agreement with the power flow simulations of the IVA and extension MITL (Fig. 4) and also of the transition region (Fig. 5). However, because of ion-electron hose instabilities, the simulations of Fig. 6 substantially underestimate the observed beam spot size.

Table I

	Beam Spot FWHM (mm)	
B_Z (T)	Experiment	IVORY Simulation
6	3.1	2.83
29	1.5	1.25

The intense electron beam produced by the SABRE foilless diode quickly produces an ion-emitting anode plasma. the ions, mostly protons, are accelerated toward the cathode with a current reduced roughly by the ratio of the ion-to-electron beam velocity (3 kA ions versus 30 kA electrons for typical SABRE parameters). The electrostatic attraction between the two beams is considerable and various forms of the two-stream instability can be excited, including sausage, hollowing, hose, and filamentation. These instabilities can cause large deflections and heating of the beam which would increase the beam spot size in the absence of a strong axial magnetic field (B_Z). Theoretical analysis and numerical simulations with IVORY[14] demonstrated the existence of these instabilities for the parameter space of the present experiment. According to simple theory and IVORY simulations, the apparent beam spot size decreases inversely with the applied magnetic field. A 30-T or higher field controls these instabilities and allows 0.5 to 0.75 mm radius beams (Fig. 7). The experimental results are in very good agreement with IVORY simulations (Table I). Figure 8 presents two time-integrated pinhole x-ray images of the beam on the anode target for two magnetic field strengths: 6 T (Fig. 8a) and 28.5 T (Fig. 8b).

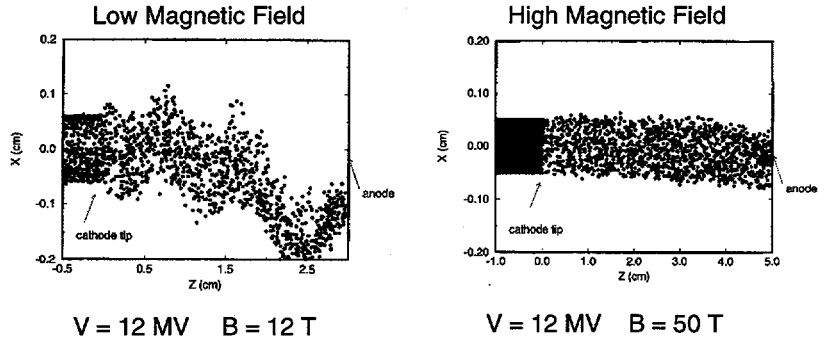

Figure 7. 3D simulations with IVORY. The higher magnetic field control the ion-electron two-stream instabilities.

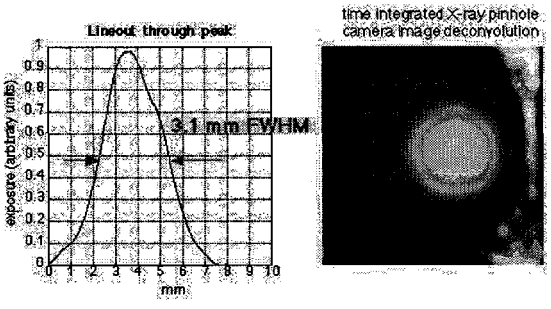

Figure 8a. Time-integrated x-ray images of the beam for B_Z = 6 T.

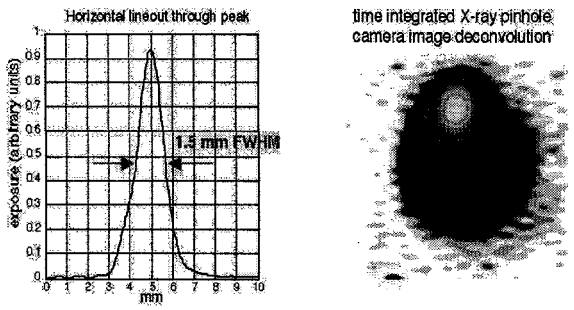

Figure 8b. Time-integrated x-ray images of the beam for B_Z = 29 T.

The time evolution of the beam profile was followed with an 8-frame x-ray framing camera. Each frame was 6-ns wide. For magnetic fields lower than 20 T, the apparent beam cross section increased with time before breaking into diverging clusters, further increasing the electron beam size. For magnetic fields closer to 30 T (28.5 T in Fig. 8), the beam profile from frame to frame remained the same, well focused with constant cross section. In Fig. 8b, it is obvious that there is an intense center core surrounded by a tenuous asymmetric halo due to cathode needle misalignment. The halo believed to be principally due to emission from the needle holder should be eliminated in a design guided by a systematic study and analysis of the transition region profile and magnetic fringe field shaping.

The beam temperature was evaluated by comparing the thermoluminescent dosimeter obtained polar diagrams with numerical simulation predictions (Fig. 9). The beam temperature is in the range $0.1 < \beta \leq 0.2$ higher than predicted without ions (Fig. 6), but in excellent agreement with simulations that include proton emission from the anode target.

The experimentally measured voltage, current, and x-ray radiation pulse are internally consistent and in full agreement with theory and numerical simulations (Figs. 4,5,6). In Fig. 10, the bremsstrahlung x-ray radiation production pulse f(t) is estimated by the semiempirical expression

$$f(t) = V(t)^{2.8} e^{-\frac{(V(t)+0.5)\beta_\perp}{.667\pi}} I(t)$$

where V is the beam voltage (MV), I is the beam current (A), and $\beta_\perp$ is the beam transverse velocity.

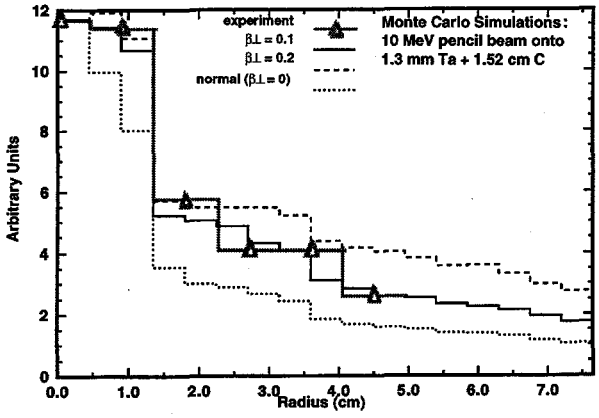

Figure 9. Dose polar map best matches $\beta_\perp$ = 0.1.

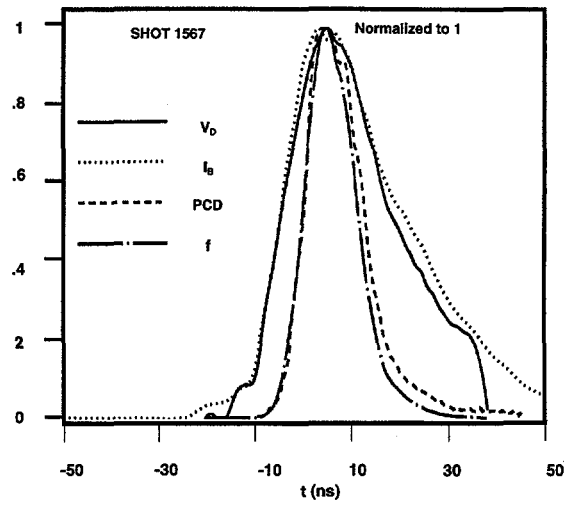

Figure 10. The experimentally measured diode voltage, current, and x-ray radiation pulse are internally consistent and in full agreement with theory and simulations.

In summary, SABRE experiments demonstrated that a magnetically immersed foilless diode driven by an inductive voltage adder can produce 1.5-mm (FWHM) electron beams. A ~ 30-T solenoidal magnetic field controlled the ion hose instability and prevented beam disruption. The experimentally measured voltage, current, x-ray dose, $\beta_\perp$, and spot size are in excellent agreement with analytical theory and numerical simulations.

HERMES-III Experiments

We currently utilize the HERMES-III accelerator to extend SABRE results to higher voltage (12 MV), longer pulse length (~ 70-ns FWHM), and higher diode magnetic field (50 T). The higher magnetic field should produce even smaller beam spot sizes of the order of 0.75-mm FWHM. The increased voltage and pulse length are required to achieve 1 kRad x-ray dose at 1 m from the Ta target.

HERMES III is larger than SABRE, having 20 inductively insulated cavities, each rated to a 1-MV maximum voltage. A number of modifications converted HERMES III from routine parameters (18 MV, 700 kA, 20 ns) to our levels (12 MV, 150 kA, 70 ns): the pulse forming line length was doubled, a new cathode electrode increased the final impedance to 110 ohms, and the Marx generators were charged to lower voltage (60 kV). The cantilevered cathode electrode is now of much smaller radius and longer (18 m). To increase its strength, continuous tapered sections were utilized instead of the stairstep design approach of previous voltage adders.[2,3,4] The outer cylinder of the extension MITL also has conical sections to reduce the radius down to SABRE size. Thus, the same magnetically immersed diode (Fig. 1) assemblies are utilized with HERMES III. In addition, a smaller, 50-T, cryogenic diode was designed and constructed (Fig. 11).

HERMES III is a very reliable accelerator and performed as expected. We produced with great reproducibility 12-MV, 150-kA, 70-ns FWHM pulses with 50-ns flat top at the output end of the long extension MITL (Fig. 12). In addition, all the pulse-forming network waveforms are in full agreement with the circuit code simulations (Fig. 13).

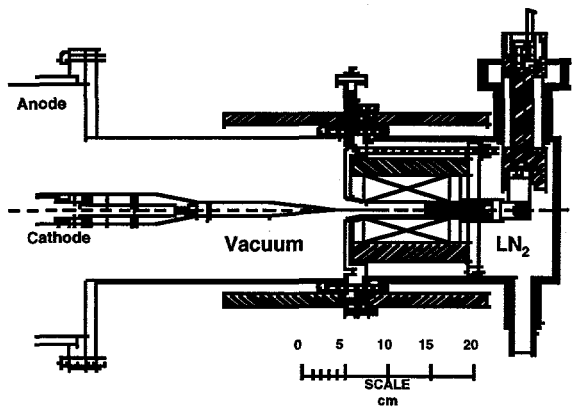

Figure 11. Schematic diagram of the 50-T cryogenic diode constructed for the HERMES-III experiments.

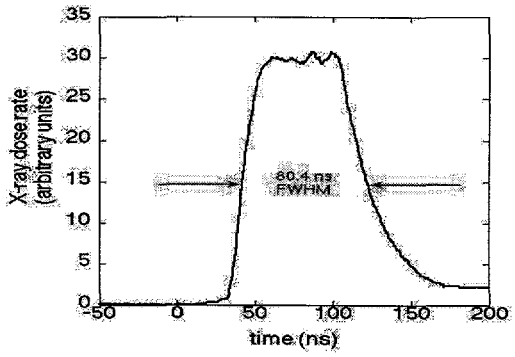

Figure 12. Bremsstrahlung x-ray radiation pulse obtained with the new cathode electrode and extension MITL. A 40-cm AK gap planar no magnetized diode was utilized for this shot.

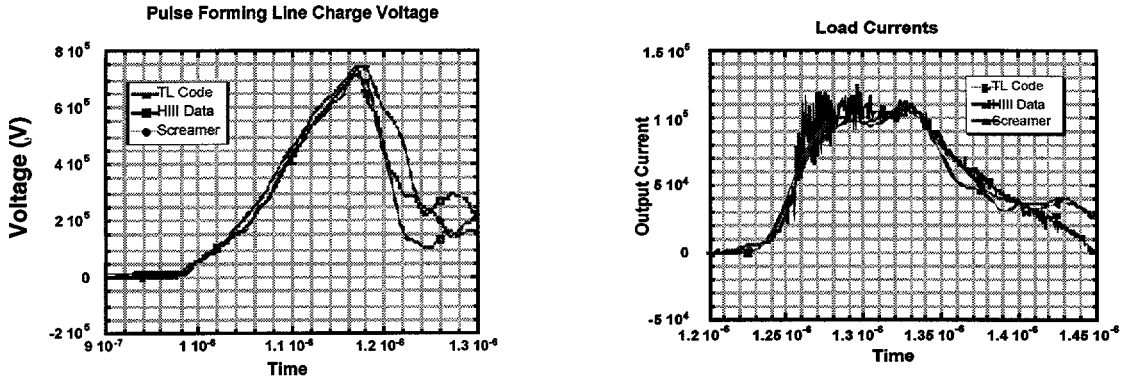

Figure 13. The waveforms calculated with SCREAMER and TL circuit codes are in very good agreement with the measured (HERMES-III) waveforms.

During SABRE experimentation, we observed a severe decrease in the diode impedance near the peak of the voltage pulse. It was attributed to a combination of a 100-kV prepulse arriving 200 ns before the main pulse and poor vacuum (1×10^{-5} torr). A flashover prepulse suppression switch and improved pumping ($< 2\times10^{-6}$ torr) solved the problem. The modified HERMES III produces a similar amplitude prepulse, and similar prepulse flashover switches were installed on the cathode electrode 30 cm upstream from the AK gap. Unfortunately, because of unexpected leaks inside the accelerator column, the initial experiments were unable to couple well to the available long pulse at constant impedance for the entire 70 ns. Figure 14 shows voltage, diode current, and diode impedance for SABRE normal operation (Fig. 14a) with prepulse flashover switch in place and good vacuum. Figure 14b presents similar HERMES-III diode parameters with the present poor vacuum (7×10^{-6} torr). At the beginning of the pulse, the impedance appears reasonable, and the first few frames of the x-ray framing camera show beam spot sizes similar to SABRE and in good agreement with simulations. It is expected that improving the vacuum on HERMES III will enable the same high-quality results as were observed on SABRE and will demonstrate immersed diode operation of full 70-ns duration with a 0.75-mm beam spot and 1 kR dose @ 1 m.

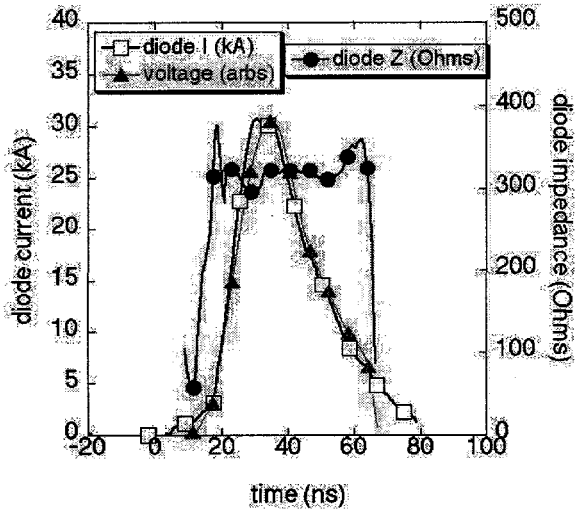

Figure 14a. A constant impedance diode shot with SABRE.

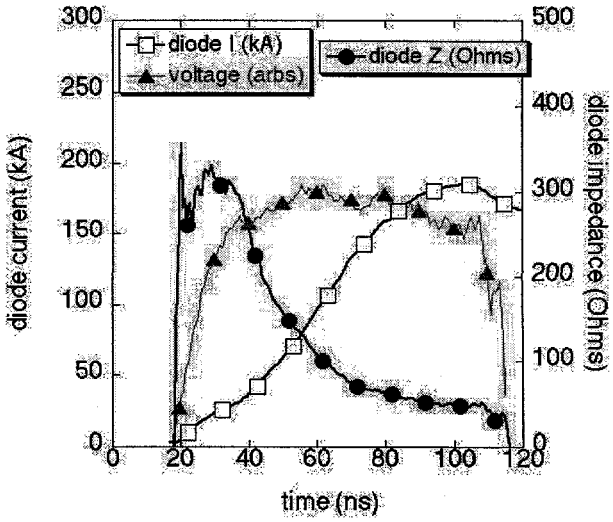

Figure 14b. The impedance of the HERMES-III diode decays with time, probably due to poor accelerator vacuum and oil contamination.

Conclusions

SABRE experiments demonstrated that an inductive voltage adder driven magnetically immersed foilless diode can successfully produce intense high-brightness electron beams of millimeter size. Ion-hose instabilities have imposed a lower spot size limit of 1.5-mm FWHM to the beam. The 50-T, HERMES-III experiments should further minimize the ion-hose effect and reduce the beam spot size to ~ 0.7-mm FWHM. In our first experimental campaign, the modified HERMES III performed superbly routinely delivering a 12-MV, 70-ns, 150-kA pulse at the end of the 18-m long MITL. However, poor vacuum inside the IVA accelerating column prevented the immersed diode from operating at full capacity. These problems are being addressed, and in the upcoming experimental campaign, we hope to achieve all the experimental goals.

Acknowledgments

This work was supported by the United States Department of Energy under Contract DE-AC04-94AL85000. Sandia is a multiprogram laboratory operated by Sandia Corporation, a Lockheed Martin Company, for the United States Department of Energy.

References

1. M. G. Mazarakis, G. T. Leifeste, R. S. Clark, C. A. Ekdahl, C. A. Frost, D. E. Hasti, D. L. Johnson, R. B. Miller, J. W. Poukey, K. R. Prestwich, S. L. Shope, and D. L. Smith, *Proc. 1987 IEEE Particle Accelerator Conf.*, Washington, DC (IEEE, New York, 1987), p. 908.
2. M. G. Mazarakis, J. W. Poukey, S. L. Shope, C. A. Frost, B. N. Turman, J. J. Ramirez, and K. R. Prestwich, *Proc. 8th Int. IEEE Pulsed Power Conf.*, San Diego, CA (IEEE, New York, 1991), p. 86.
3. J. Corley, J. A. Alexander, P. J. Pankuch, C. E. Heath, D. L. Johnson, J. J. Ramirez, and G. J. Denison, *Proc. 8th Int. IEEE Pulsed Power Conf.*, San Diego, CA (IEEE, New York, 1991), p. 920.
4. J. J. Ramirez, K. R. Prestiwch, E. L. Burgess, J. P. Furaus, R. A. Hamil, D. L. Johnson, T. W. L. Sanford, L. E. Seamons, L. X. Schneider, and G. A. Zawadzkas, *Proc. 6th Int. IEEE Pulsed Power Conf.*, Arlington, VA (IEEE, New York, 1987), p. 294.
5. T. M. Martin, *IEEE Trans. Nucl. Sci.* **NS-16**, 59 (1969).
6. J. J. Ramirez, J. P. Corley, and M. G. Mazarakis, *Proc. 5th Int. Conf. on High-Power Particle Beams*, San Francisco, CA (Physics International, San Leandro, CA, 1983), p. 256.
7. R. B. Miller, K. R. Prestwich, J. W. Poukey, B. G. Epstein, J. R. Freeman, A. W. Sharpe, W. K. Tucker, and S. L. Shope, *J. Appl. Phys.* **52**, 1184 (1981).
8. D. E. Hasti, J. J. Ramirez, P. D. Coleman, C. W. Huddle, A. W. Sharpe, L. L. Torrison, *Proc. 5th Int. IEEE Pulsed Power Conf.*, Arlington, VA (IEEE, New York, 1985), p. 147.
9. L. M. Friedman and M. Ury, *Rev. Sci. Instrum.* **41**, 1334 (1970).
10. J. M. Creedon, *J. Appl. Phys.* **48** (3), 1070 (1977).
11. N. Christophilos, R. E. Hester, W. A. S. Lamb, D. D. Reagan, W. A. Sherwood, and R. E. Wright, *Rev. Sci. Instrum.* **35** (7), 886 (1964).
12. J. W. Poukey, M. G. Mazarakis, C. A. Frost, and J. J. Ramirez, *Proc. IEEE Particle Accelerator Conf.*, San Francisco, CA (1991), p. 3059.
13. M. G. Mazarakis, J. W. Poukey, C. A. Frost, D. L. Johnson, S. L. Shope, J. A. Halbleib, K. R. Prestwich, B. N. Turman, and I. Smith, *Proc. IEEE Int. Conf. on Plasma Science*, Tampa, FL (1992), p. 104.
14. D. B. Seidel, M. L. Kiefer, R. S. Coats, T. D. Pointon, J. P. Quintenz, and W. A. Johnson, *Proc. CP90 Europhysics Conf. on Computational Physics*, Singapore (World Scientific, Singapore, 1991), p. 475.

DISCLAIMER